Supplementary Information

Three Different Metal-Organic Frameworks Derived From One-Pot Crystallization and Their Controllable Synthesis

Chuanlei Zhang, Yanle Li, Ting Wang, Zemin Ju, Hegen Zheng,* Jing Ma*

Contents

1. Experimental section.

Materials and measurements. Reagents and solvents employed were commercially available. Ligand H_3L was prepared by the literature methods.[1] DPDP ligand was prepared on the basis of palladium-catalyzed cross-coupling reactions. IR absorption spectra of the compounds **1** - **3** were recorded in the range of 400–4000 cm^{-1} on a Nicolet (Impact 410) spectrometer with KBr pellets (5 mg of sample in 500 mg of KBr). C, H and N analyses were carried out with a Perkin Elmer 240C elemental analyzer. Powder X-ray diffraction (PXRD) measurements were performed on a Bruker D8 Advance X-ray diffractometer using Mo-K_α radiation (λ = 0.71073 Å), in which the X-ray tube was operated at 40 kV and 40 mA. The as-synthesized samples were characterized by thermogravimetric analysis (TGA) on a Perkin Elmer thermogravimetric analyzer Pyris 1 TGA up to 1023 K using a heating rate of 10 K min^{-1} under N_2 atmosphere. Direct current (DC) magnetic susceptibility and magnetization measurements were carried out on a Quantum Design MPMS-XL7 superconducting quantum interference device (SQUID) magnetometer.

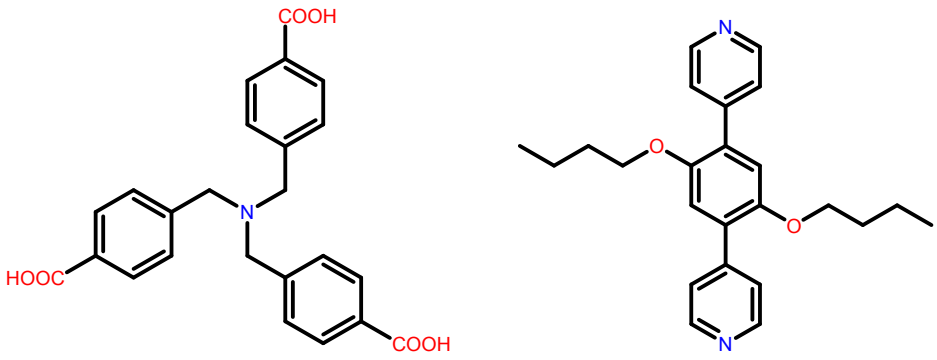

H_3L DPDP

Scheme S1. Tricarboxylic acid and DPDP ligand.

Synthesis of complexes 1-3. A mixture of DMA/CH_3OH (8 ml: 3/5) containing the H_3L (41.9 mg, 0.1 mmol), DPDP (37.6 mg, 0.1 mmol) and $Co(NO_3)_2 \cdot 6H_2O$ (29.1 mg, 0.1 mmol) was mixed in a Teflon vessel within the autoclave. The vessel was heated at 95 °C for 72 h and then cooled to room temperature. Large quantities of crystals **1** (purple rice-shaped), **2** (pink block-shaped), and **3** (crimson strip-shaped) were obtained and crystals were filtered off, washed with mother liquid, and dried under

ambient conditions. The crystals were separated by hand picking and yield of the reaction were ca. 10% in 1, 20% in 2, 20% in 3 based on H_3L. Elemental analysis calcd. for $C_{72}H_{64}Co_3N_4O_{14}$ (**1**): C, 62.34; H, 4.62; N, 4.04, Found: C, 62.54; H, 4.73; N, 4.12; calcd. for $C_{48}H_{47}CoN_3O_8$ (**2**): C, 67.61; H, 5.51; N, 4.94, Found: C, 68.04; H, 5.44; N, 4.86; calcd. for $C_{60}H_{65}CoN_4O_{11}$ (**3**): C, 66.85; H, 6.04; N, 5.20, Found: C, 66.70; H, 6.12; N, 5.13. The IR spectra of the corresponding complexes are shown in the Fig. S11-13.

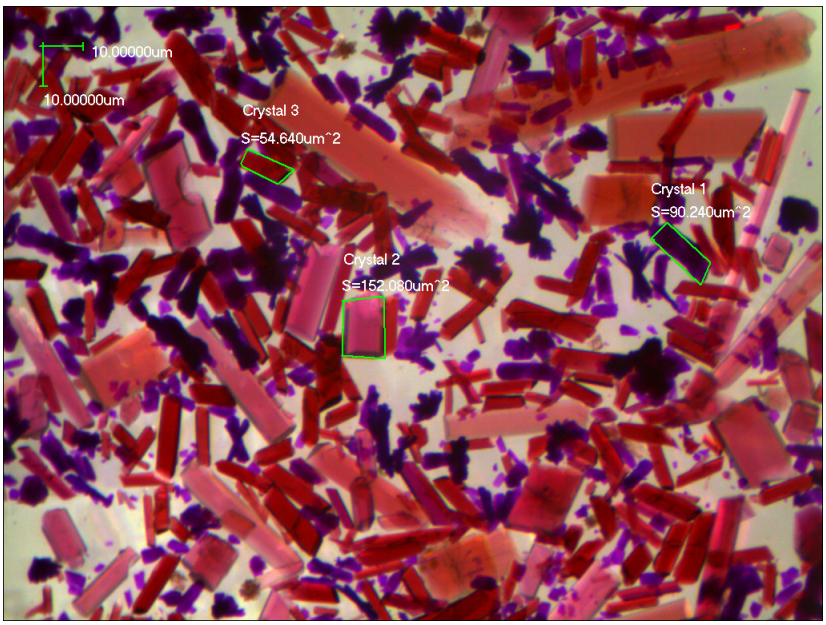

Fig. S1 The optical microscope photographs of complexes **1-3**.

X-ray crystallography. Single crystals of complexes **1-3** were tested on a Bruker SMART APEX CCD diffractometer using graphite monochromated Mo Kα radiation (λ = 0.71073 Å) at 296 K. From the data reduction to the structure determination, the follow procedures were used: the International Tables for X-ray Crystallography,[2] SAINT,[3] SADABS,[4] XPREP,[5] SHELXTL-97[6] and SHELXTL-97 program[7] package.

Table S1. Crystal data and structural refinements parameters of complexes **1-3**.

Complexes	**1**	**2**	**3**
Empirical formula	$C_{72}H_{64}Co_3N_4O_{14}$	$C_{48}H_{47}CoN_3O_8$	$C_{60}H_{65}CoN_4O_{11}$
Formula weight	1386.06	852.82	1077.09
Crystal system	Monoclinic	Triclinic	Triclinic

Space group	*C*2/*c*	$P\bar{1}$	$P\bar{1}$
a / Å	26.758(9)	12.848(3)	10.6129(4)
b / Å	10.635(4)	14.185(3)	14.9365(6)
c / Å	29.565(8)	15.785(3)	18.7658(8)
α / °	90	114.870(3)	108.9870(10)
β/ °	116.76(3)	97.126(4)	92.3480(10)
γ/ °	90	109.338(3)	106.1340(10)
V / Å^3	7503(4)	2343.4(9)	2673.70(19)
Z	4	2	2
D_{calcd} / g cm^{-3}	1.227	1.209	1.338
μ / mm^{-1}	0.716	0.419	0.387
F(000)	2868	894	1136
θ min-max / °	1.71, 25.00	1.49, 26.02	1.16, 27.51
Tot., uniq. data	20350, 6594	18858, 9111	18459, 12220
R(int)	0.1262	0.0495	0.0347
Nres, Npar	239, 376	279, 543	333, 685
R_1, wR_2 [$I > 2\sigma(I)$]	0.0634, 0.1193	0.0583, 0.1549	0.0608, 0.1484
GOF on F^2	1.003	1.037	1.004
Min. and max resd dens (e·Å^{-3})	-0.448, 0.863	-0.420, 0.582	-0.563, 1.203

Table S2. Selected Bond Lengths (Å) and Angles (deg) for Complexes **1-3**.

Complex **1**			
Co(1)-O(4)#3	1.965(4)	Co(1)-O(1)	1.972(5)
Co(1)-O(5)#4	1.988(4)	Co(1)-N(1)	2.063(5)
Co(1)-O(6)#4	2.316(4)	Co(2)-O(2)	2.014(4)

Co(2)-O(4)#1	2.025(7)	Co(2)-O(1)#4	2.050(7)
Co(2)-O(2)#5	2.014(4)	Co(2)-O(3)#3	2.054(4)
Co(2)-O(6)#7	2.138(4)	O(4)#3-Co(1)-O(1)	135.0(2)
O(4)#3-Co(1)-O(5)#4	108.7(2)	O(1)-Co(1)-O(5)#4	109.84(18)
O(4)#3-Co(1)-N(1)	90.1(2)	O(1)-Co(1)-N(1)	98.4(2)
O(5)#4-Co(1)-N(1)	109.3(2)	O(4)#3-Co(1)-O(6)#4	87.22(18)
O(1)-Co(1)-O(6)#4	92.49(17)	O(5)#4-Co(1)-O(6)#4	59.89(16)
N(1)-Co(1)-O(6)#4	167.0(2)	O(2)-Co(2)-O(3)#3	92.08(18)
O(2)-Co(2)-O(3)#6	87.92(18)	O(2)#5-Co(2)-O(3)#6	92.08(18)
O(3)#3-Co(2)-O(3)#6	180.0	O(2)-Co(2)-O(6)#7	90.65(18)
O(2)#5-Co(2)-O(6)#7	89.35(18)	O(3)#3-Co(2)-O(6)#7	86.78(18)
O(3)#6-Co(2)-O(6)#7	93.22(18)		
Complex **2**			
O(4)-Co(1)#1	2.027(2)	Co(1)-O(3)#3	2.037(2)
O(3)-Co(1)#2	2.037(2)	Co(1)-O(1)	2.090(2)
Co(1)-O(4)#1	2.026(2)	Co(1)-N(2)#4	2.134(2)
Co(1)-N(1)	2.190(3)	Co(1)-O(2)	2.367(2)
N(2)-Co(1)#5	2.134(2)	O(4)#1-Co(1)-O(1)	96.79(10)
O(4)#1-Co(1)-O(3)#3	103.08(9)	O(3)#3-Co(1)-O(1)	158.11(9)
O(4)#1-Co(1)-N(2)#4	93.86(10)	O(3)#3-Co(1)-N(2)#4	95.45(10)
O(1)-Co(1)-N(2)#4	92.25(10)	O(4)#1-Co(1)-N(1)	87.79(9)
O(3)#3-Co(1)-N(1)	87.07(9)	O(1)-Co(1)-N(1)	84.59(9)
N(2)#4-Co(1)-N(1)	176.59(10)	O(4)#1-Co(1)-O(2)	153.72(9)
O(3)#3-Co(1)-O(2)	100.50(9)	O(1)-Co(1)-O(2)	58.31(9)
N(2)#4-Co(1)-O(2)	95.27(9)	N(1)-Co(1)-O(2)	81.97(9)
Complex **3**			

Co(1)-O(10)	2.073(2)	Co(1)-O(6)#1	2.091(2)
Co(1)-O(1)	2.129(2)	Co(1)-N(1)	2.192(3)
Co(1)-N(2)	2.201(3)	Co(1)-N(3)	2.208(2)
O(10)-Co(1)-O(6)#1	86.52(9)	O(10)-Co(1)-O(1)	89.83(9)
O(6)#1-Co(1)-O(1)	176.21(9)	N(2)-Co(1)-N(3)	171.11(10)
N(1)-Co(1)-N(3)	89.17(10)	O(1)-Co(1)-N(3)	87.63(9)
O(6)#1-Co(1)-N(3)	91.37(9)	O(10)-Co(1)-N(3)	90.58(10)
N(1)-Co(1)-N(2)	82.09(10)	O(1)-Co(1)-N(2)	91.00(10)
O(6)#1-Co(1)-N(2)	90.55(10)	O(10)-Co(1)-N(2)	98.21(10)
O(1)-Co(1)-N(1)	91.64(10)	O(6)#1-Co(1)-N(1)	92.01(10)
O(10)-Co(1)-N(1)	178.50(10)		

Symmetry Codes: for **1:** 1# = $x - 1/2, y + 1/2, z$; #2 = $- x + 1/2, - y - 1/2, - z$; #3 = $x, - y + 1, z - 1/2$; #4 = $x + 1/2, y - 1/2$, z; #5 = $- x + 1, - y + 1, - z, - z + 1/2$; #6 = $- x + 1, y, - z + 1/2$; #7 = $- x + 1/2, - y + 3/2, -$ z. for **2:** #1 = $– x + 1, – y + 3, –z + 1$; #2 = $x, y + 1, z + 1$; #3 = $x, y - 1, z - 1$; #4 = $x + 1, y + 1, z$; #5 = $x - 1, y - 1, z$. for **3:** #1 = $x + 1, y + 1, z$

2. Structural drawing for complexes 1-3.

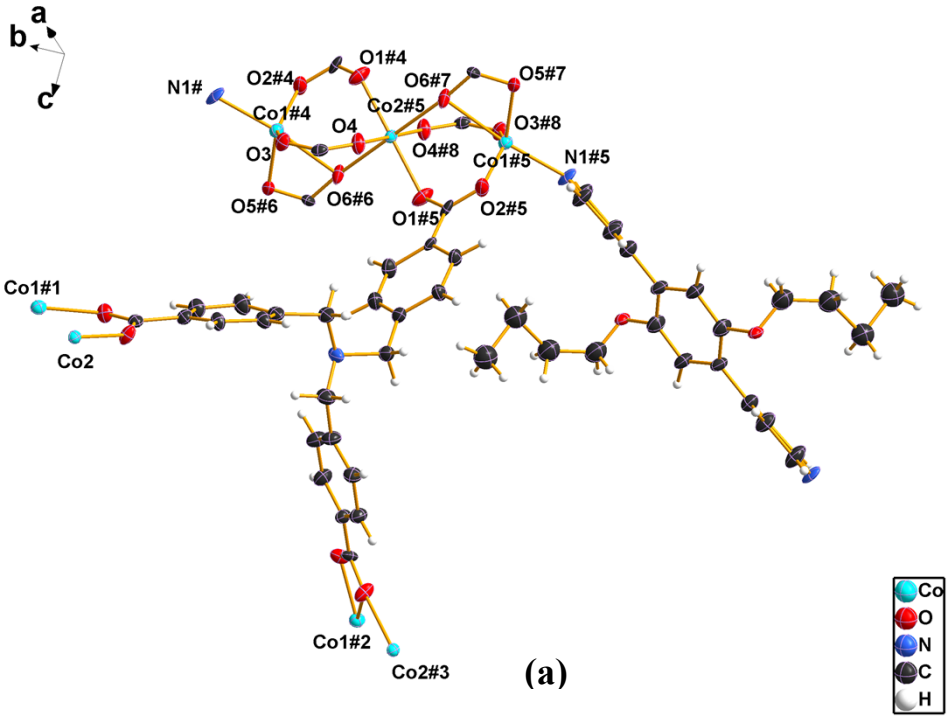

(a)

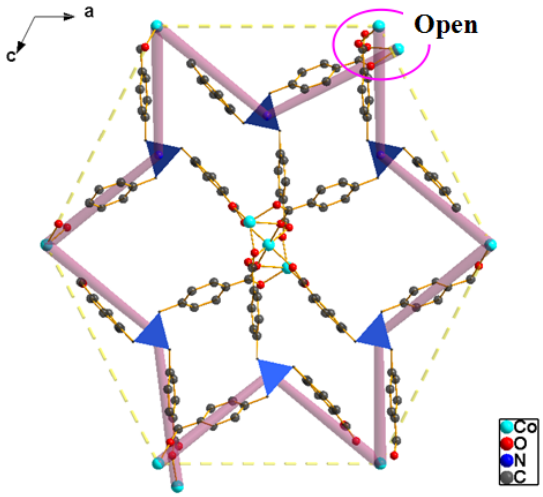

(b)

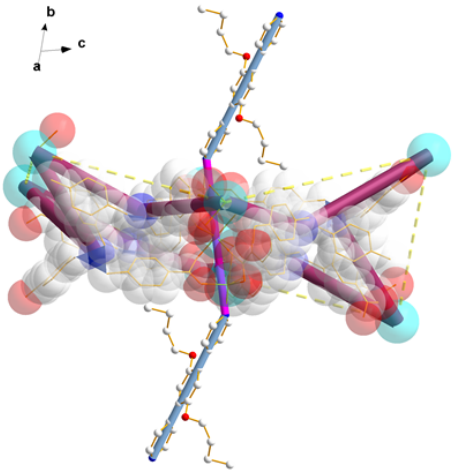

(c)

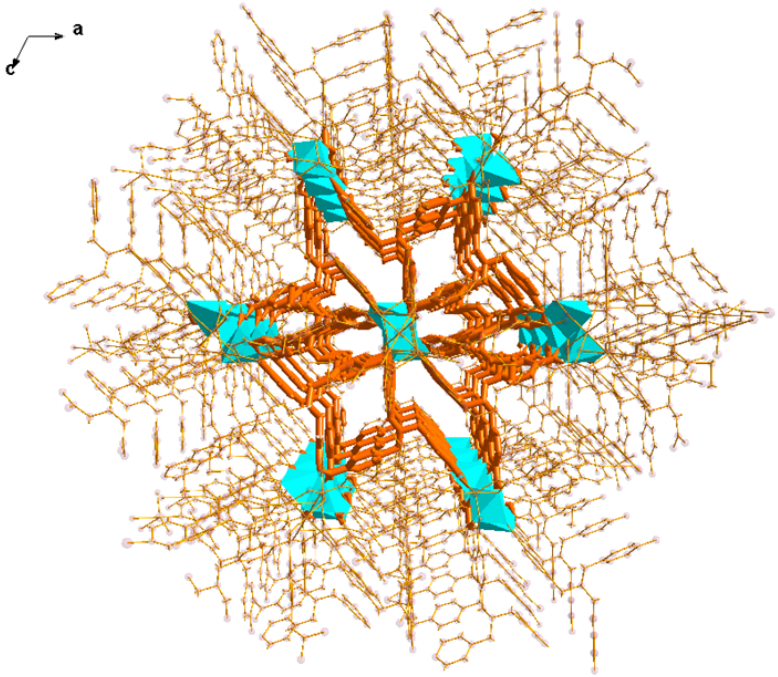

(d)

(e)

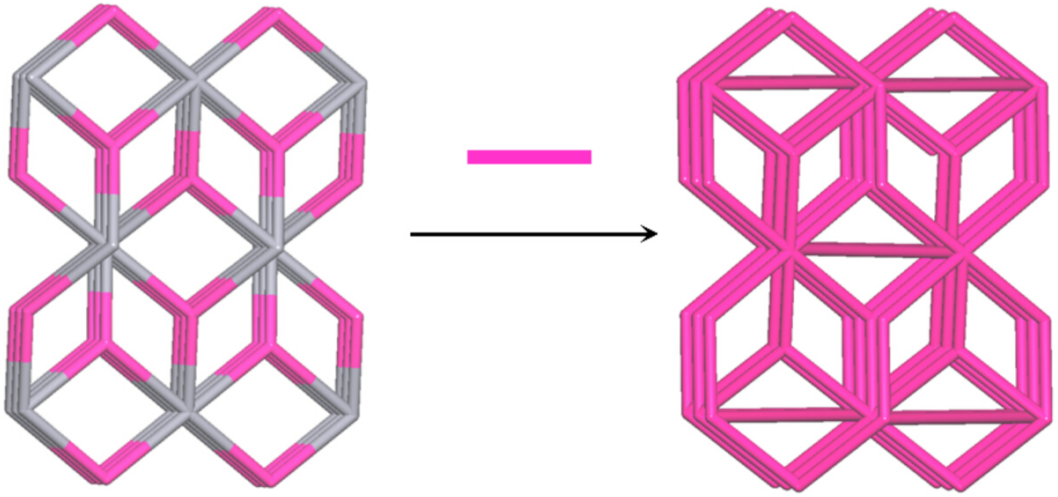

(f)

Fig. S2 (a) Coordination environment of **1** with 30% ellipsoid probability. Symmetry code: #1 = 0.5 − *x*, 1.5 − *y*, 1 − *z*; #2 = − *x*, 1 − *y*, 1 − *z*; #3 = − 0.5 + *x*, − 0.5 + *y*, *z*; #4 = − 0.5 + *x*, 1.5 − *y*, − 0.5 + *z*; #5 = − *x*, *y*, 0.5 − *z*; #6 = − 0.5 + *x*, 0.5 + *y*, *z*; #7 = − *x*, 1 − *y*, − *z*; #8 = − 0.5 − *x*, 1.5 − *y*, − *z*. (b) The open hexagonal ring constructed by six L^{3-} ligands and the entrosymmetric trinuclear cobalt unit. (c) The coordination of DPDP ligands from up and down positions of the ring. (d) A perspective of 3D framework along the *b* axis; (e) The 3D **flu-3,6-C2/c** framework formed by trinuclear cobalt unit and L^{3-} ligands. (f) New topology of **1** constructed by **flu-3,6-C2/c** and DPDP linkers.

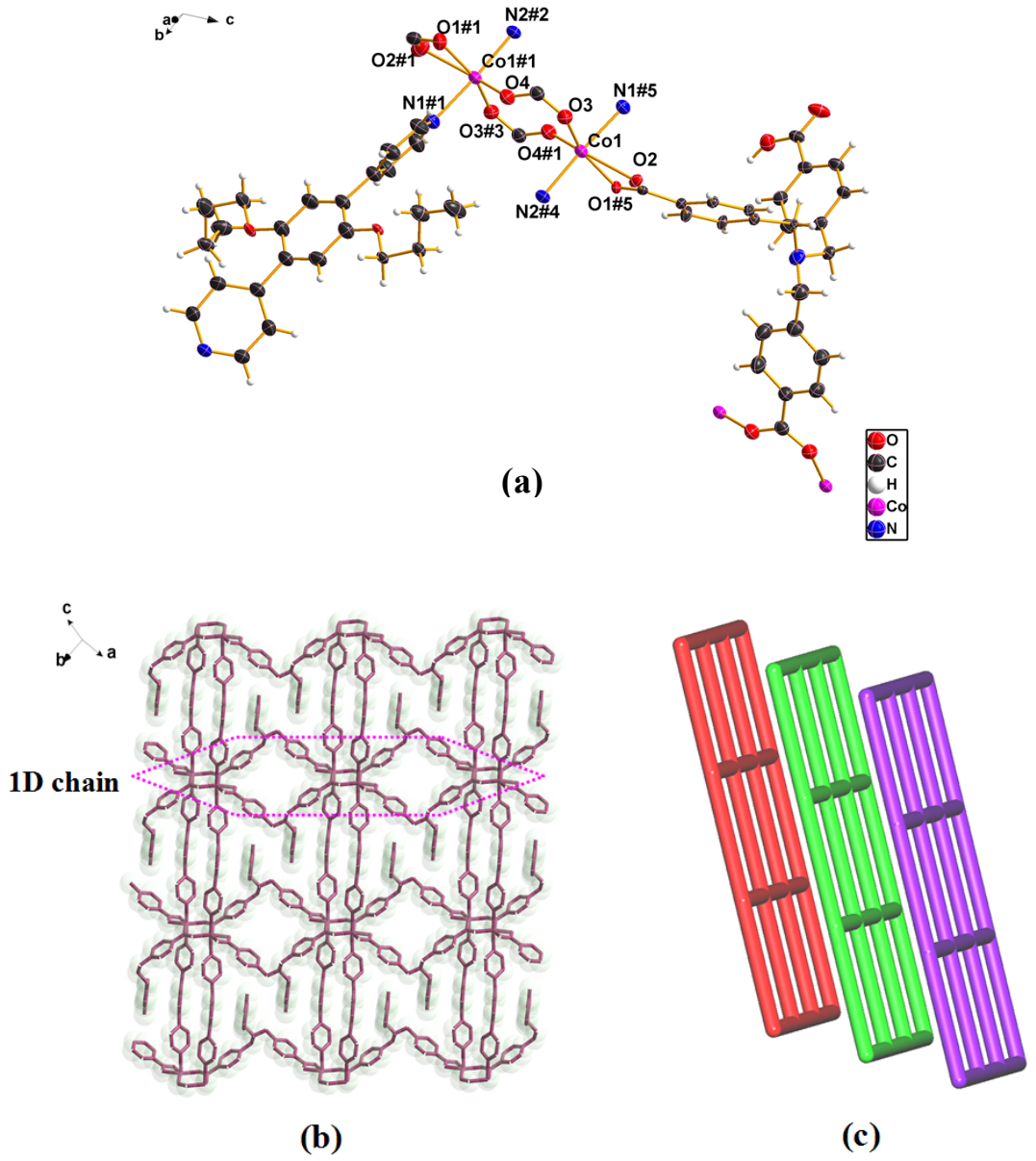

Fig. S3 (a) Coordination environment of **2** with 30% ellipsoid probability. Symmetry code: #1 = 1 − *x*, 3 − *y*, 1 − *z*; #2 = − *x*, 2 − *y* , 1 – *z*; #3 = 1 − *x*, 4 − *y*, 2 − *z*; #3 = 1 + *x*, 2 + *y*, 1 + *z*; #5 = + *x*, 1 + *y*, 1 + *z*. (b) 2D network with an infinite 1D double chain in **2**. (c) Schematic representation of an **sql** net for 2.

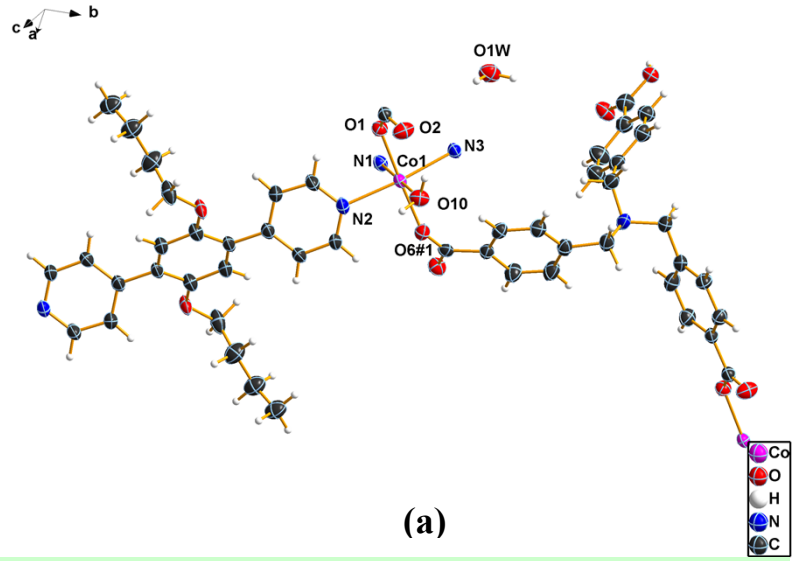

(a)

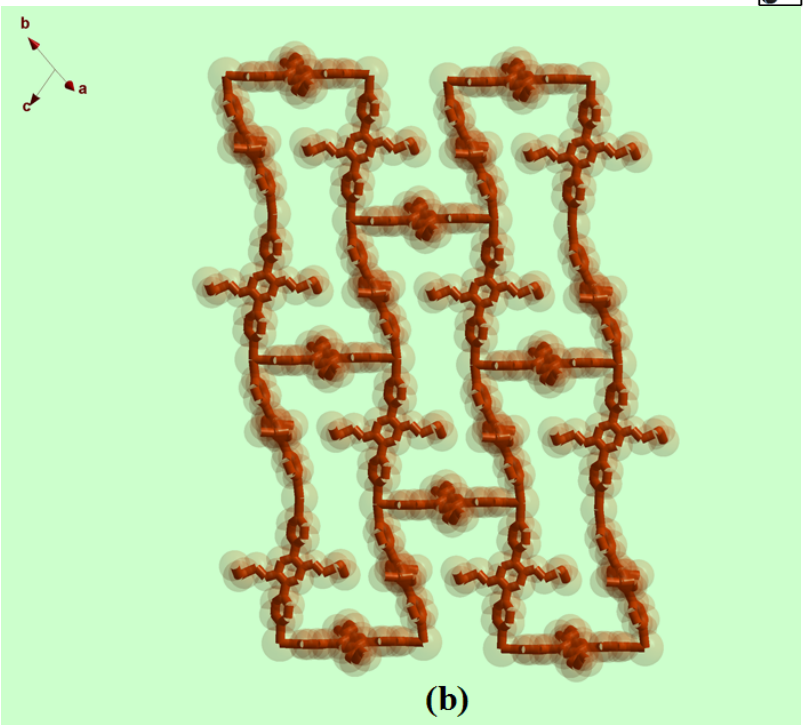

(b)

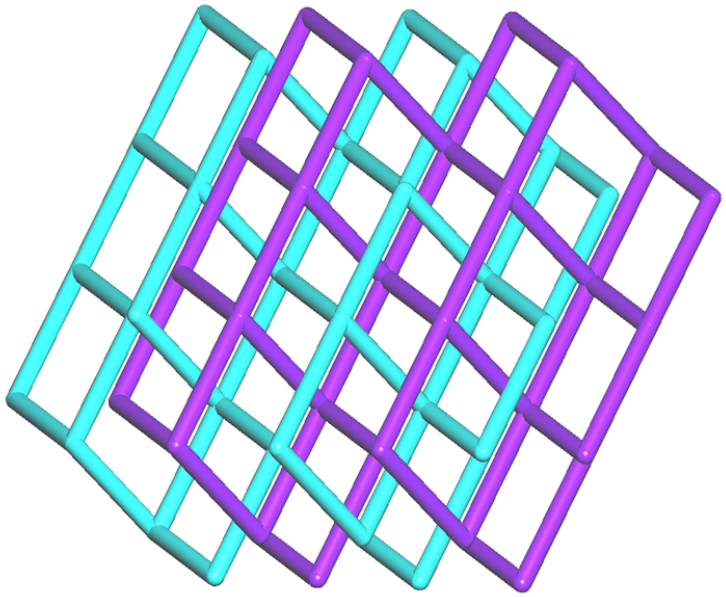

(c)

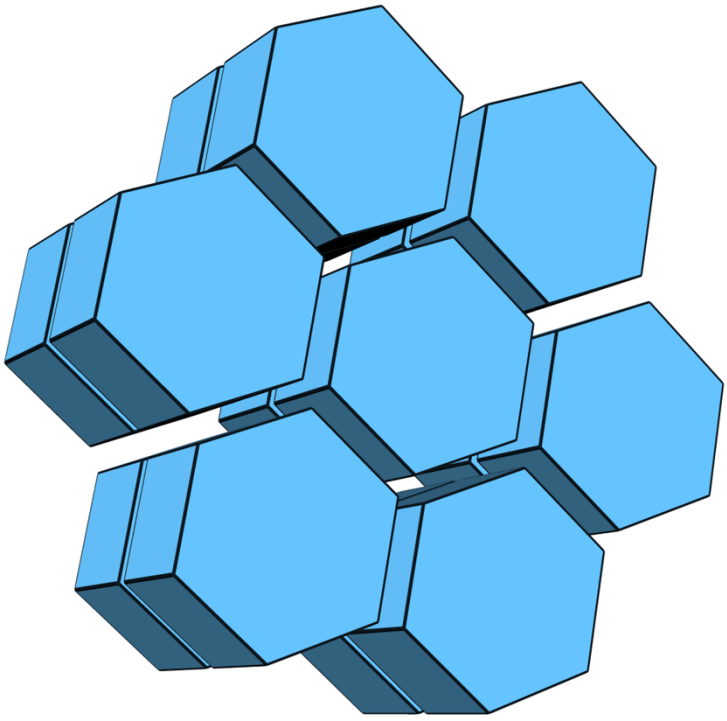

(d)

Fig. S4 (a) Coordination environment of **3** with 30% ellipsoid probability. (b) The 2D layered structure formed by DPDP linkers and Co^{2+} ions, (c) A view of 2-fold **bnn** topology. (d) Topological features of the compound displayed by tiling.

3. Powder X-ray diffraction patterns of complexes 1-3.

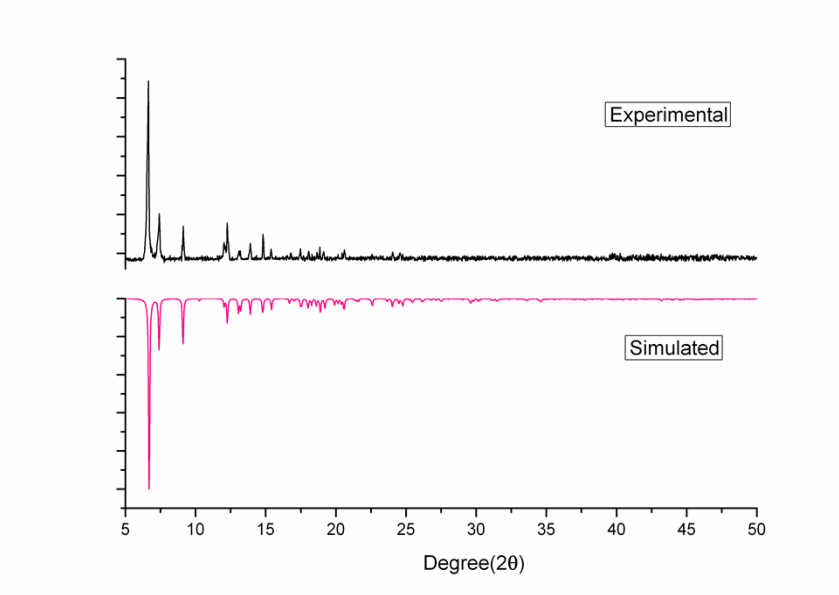

Fig. S6 Powder X-ray diffraction patterns of complex **1**

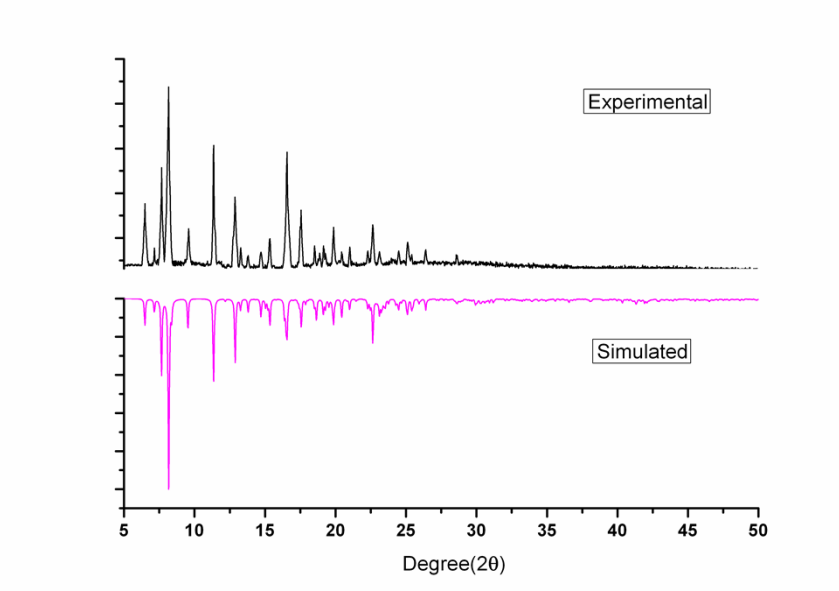

Fig. S7 Powder X-ray diffraction patterns of complex **2**

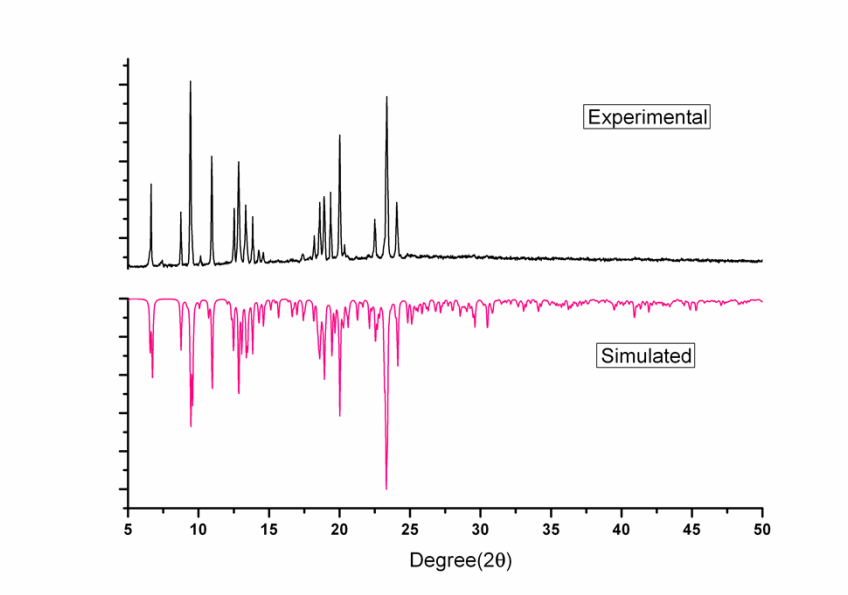

Fig. S8 Powder X-ray diffraction patterns of complex **3**

4. IR spectra of complexes 1-3 and related ligands.

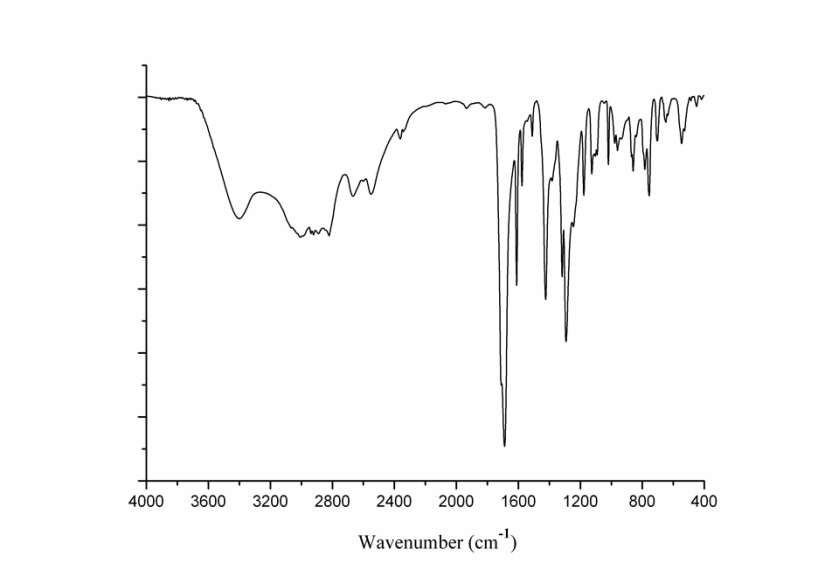

Fig. S9 IR spectra of H_3L ligand

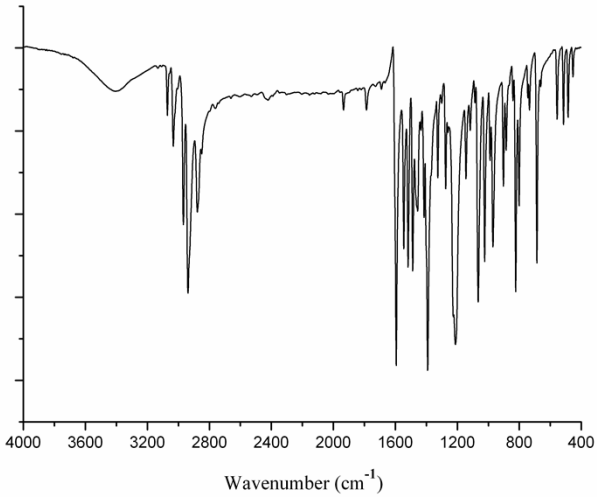

Fig. S10 IR spectra of DPDP ligand

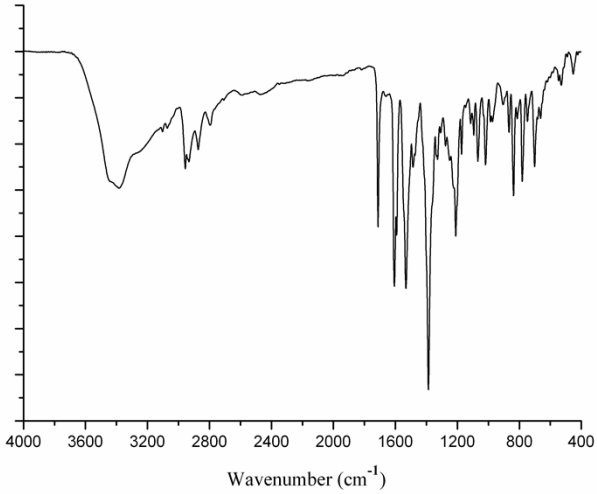

Fig. S11 IR spectra of complex **1**

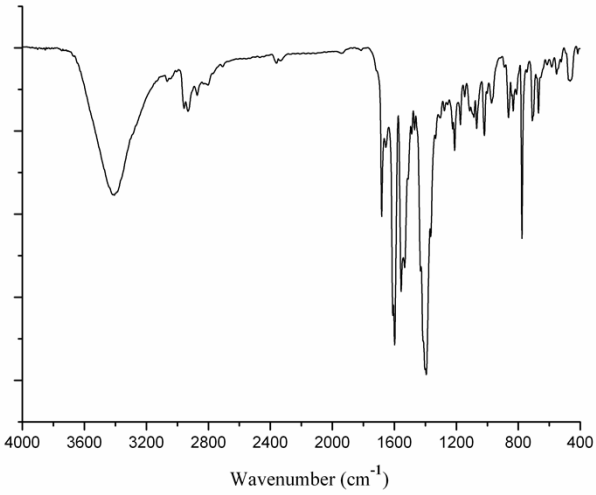

Fig. S12 IR spectra of complex **2**

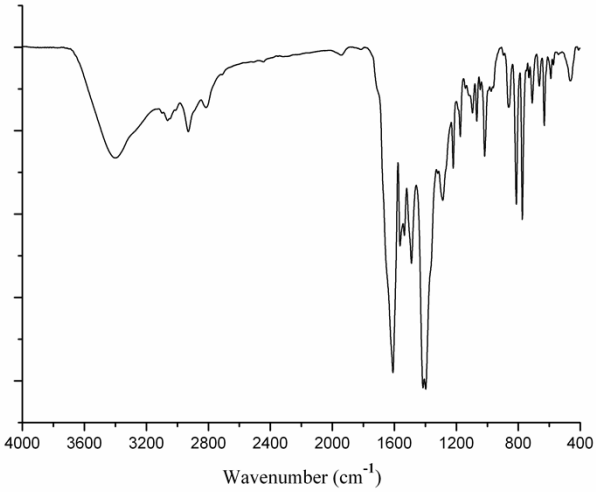

Fig. S13 IR spectra of complex **3**

5. The TGA diagrams of complexes 1 - 3.

To estimate the stability of the crystal structures, their thermal behaviors were studied by TGA (Figure S14). For complex **1**, the TG curve shows that its coordination framework can be stable to about 380 °C. Then the framework starts to decompose. For complex **2**, from 250 °C, the TG curve presents a rapid weight loss as the burning of the organic ligands, at the same time accompanied by the collapse of the skeleton. The TG curve of **3** shows a weightlessness 3.51% before 150 °C, is attributed to the loss of lattice and coordinated H_2O molecules (calcd 3.34%), then the curve transforms into a plateau region. After 250 °C, a rapid weight loss is observed, which attributes to the decomposition of coordination framework.

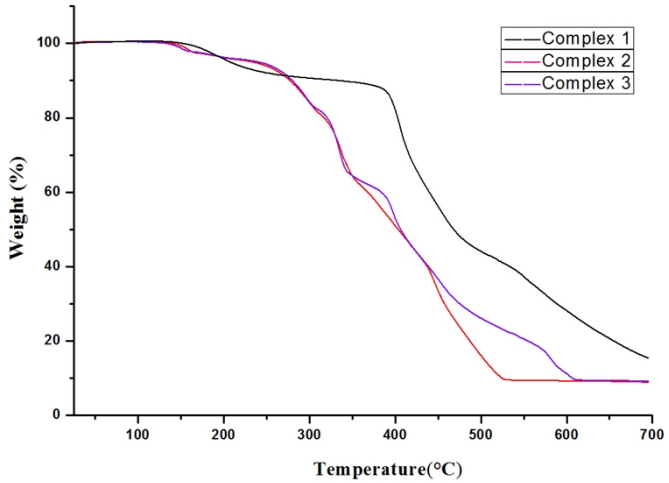

Fig. S14 The TGA diagrams of complexes **1** – **3**

6. The UV–visible spectra of complexes 1 - 3.

Considering the differences of three kinds of crystals in color, we conducted the solid state UV adsorption test. The UV–vis absorption spectra of complexes **1-3** were carried out in the crystalline state at room temperature (Figure S15). Three complexes exhibit two absorption bands between 250 and 650 nm, one band in the range of 250–425 nm can be ascribed to π–π* transitions of the ligand, the other wide band from 450 to 650nm can be considered as the spin–allowed d–d electronic transitions of the d^7 (Co^{2+}) cation. The difference in absorption intensity and the second absorption band shows that three kinds of complexes are different on color.

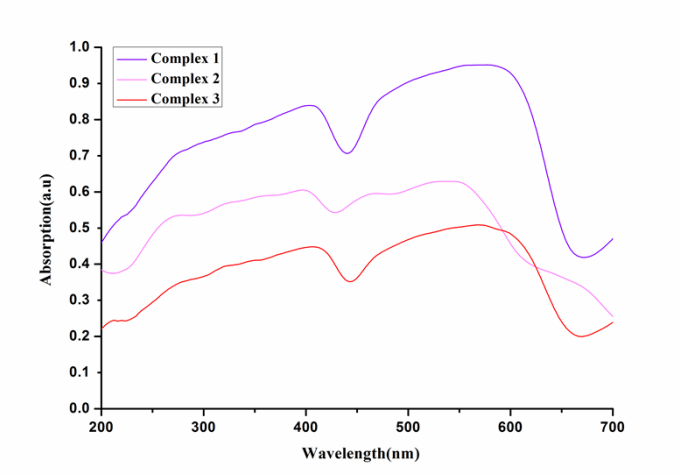

Fig. S15 The UV–vis spectra of complexes **1-3**

7. Magnetic properties of complexes 1-3.

The general spin Hamiltonian applied for linear trinuclear Co^{II} complex **1**:

$$\hat{H} = g\beta(\hat{S}_1+\hat{S}_2+\hat{S}_3)\cdot B+\hat{S}_1\cdot D_1\cdot\hat{S}_1+\hat{S}_2\cdot D_2\cdot\hat{S}_2 + \hat{S}_3\cdot D_3\cdot\hat{S}_3-J\,\hat{S}_1\cdot\hat{S}_2-J\,\hat{S}_2\cdot\hat{S}_3 \quad (1)$$

The good fit of the data is: J = + 0.034 cm^{-1}, $D_{1,3}$ = −22.1 cm^{-1}, D_2 = 18.5 cm^{-1}, g = 2.06.

The general spin Hamiltonian applied for entrosymmetric dinuclear Co^{II} complex **2**:

$$\hat{H} = g\beta(\hat{S}_1+\hat{S}_2)\cdot B+\hat{S}_1\cdot D_1\cdot\hat{S}_1+\hat{S}_2\cdot D_2\cdot\hat{S}_2-J\,\hat{S}_1\cdot\hat{S}_2$$

(2)

The good fit of the data is: J = − 0.0444 cm^{-1}, $D_1 = D_2$ = 21.104 cm^{-1}, g = 2.33.

The general spin Hamiltonian applied for mononuclear Co^{II} complex **3**:

$$H = D(\hat{S}_z{}^2-S(S+1)/3)+E(\hat{S}_x{}^2-\hat{S}_y{}^2)+\mu_B(g_x\,\hat{S}_x\,B_x+g_y\,\hat{S}_y\,B_y+g_z\,\hat{S}_z\,B_z)$$

(3)

The good fit of the data is: D = + 35.18 cm^{-1}, E = − 1.12 cm^{-1}, $g_x = g_y$= 2.25, g_z = 2.67.

8. Computational methods.

All calculations were performed with the Gaussian09 program package.[8] The optimizations and single point energy calculations were carried out at DFT M06-2X [9]

level. For nonmetal elements, we made use of the standard 6-31G basis sets. For metals Co, the effective core potentials (ECPs) with double-ζ valence basis sets (LanL2DZ) were used.[10] For complexes, we only calculated single point energy, and structures were obtained from crystal structures which were from experiment.

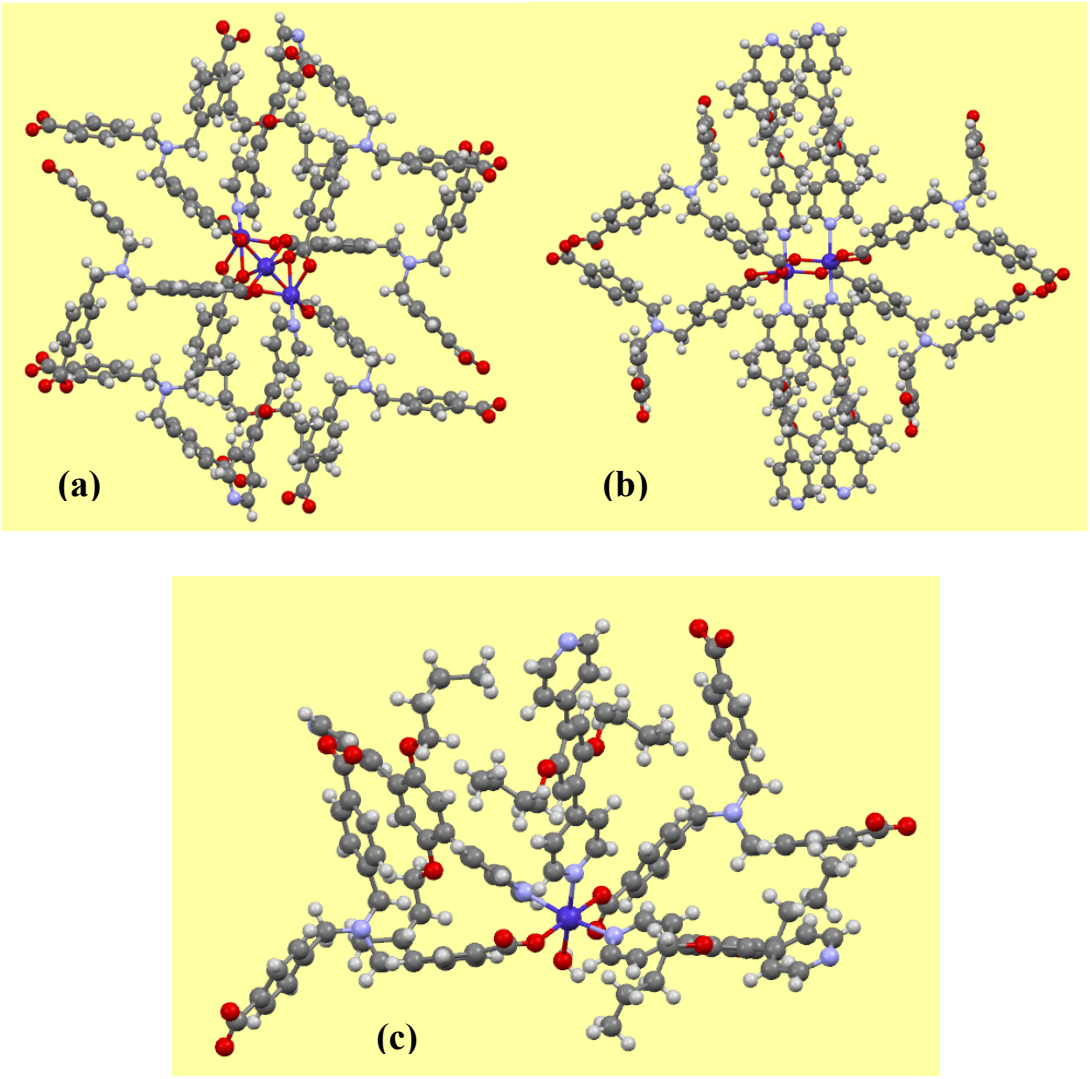

Fig. S16 The DFT computational models of structures **1**-**3**.

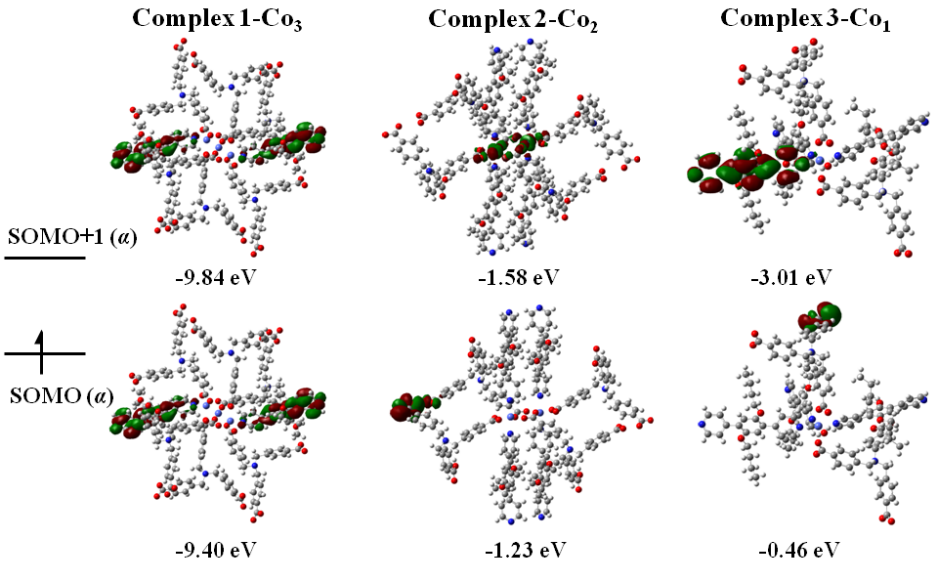

Fig. S17 Frontier molecular orbitals as well as their orbital energies calculated at B3LYP/LANL2DZ level for complexes **1-3**.

Table S3. Comparison of the ground state energies and the gaps of frontier molecular orbital energy for three different structures calculated at B3LYP/LANL2DZ level

Compounds / Energy	L^{3-}	DPDP	H_2O	Co	Complex **1**	Complex **2**	Complex **3**
Relative ground state energy $\times 10^5$ [kcal/mol]	−8.98	−7.42	−0.48	−0.9	−71.5	−67.6	−41.7
Gaps of frontier molecular orbital energy [eV]					0.44	0.35	2.55
Binding energy$\times 10^4$ [kcal/mol]					−0.94	−2.00	−1.38

The computational strategies for binding energy are as follows:

For Complex 1

$$E_{\text{Binding energy}} = E_{\text{Complex 1}} - (6 \times E_{\text{L}} + 2 \times E_{\text{DPDP}} + 3 \times E_{\text{Co}})$$

For Complex 2

$$E_{\text{Binding energy}} = E_{\text{Complex 2}} - (4 \times E_{\text{L}} + 4 \times E_{\text{DPDP}} + 2 \times E_{\text{Co}})$$

For Complex 3

$$E_{\text{Binding energy}} = E_{\text{Complex 3}} - (2 \times E_{\text{L}} + 3 \times E_{\text{DPDP}} + E_{\text{Co}} + E_{\text{H2O}})$$

9. Optimal experiment for purifing one-component crystals of complexes 1-3.

All optimization experiments were carried out at 95 °C with total amount of solvent of 8.0 ml.

Table S4. Summary of the product isolated in different solvent systems at 95 °C

Solvent / Ratio	DMA/CH_3OH	DMF/CH_3OH	DMA/CH_3CN	DMA/H_2O	Solvent / Ratio	DMA/ CH_3OH /H_2O	DMA/ CH_3CN /H_2O
0/8	powder	powder	powder	powder	**0/4/4**	powder	powder
1/7	1+2+3+ impurities	1+2+3+ impurities	1+2+3+ impurities	2+3+impurities	**1/2/5**	[1+2] few + impurities	1+ impurities
2/6	1+2+3+ impurities	1+2+3+ impurities	1+2+3+ impurities	2+3+impurities	**1/3/4**	1+2 impurities	**[1] few**
3/5	**[1+2+3] many**	**[1+2+3] many**	1+2+3	**[2+3] many**	**1/5/2**	[1+2] few	[1+2] few
4/4	[1+2+3] many	[1+2+3] many	1+2+[3] trace	1+[2+3] few	**2/2/4**	[1+2] trace +3	[1+2] few
5/3	[1+2+3] few	[1+2+3] few	**[1+2] many**	1+[2] trace+3	**2/3/3**	[3] few	[1] few + 2
6/2	[1+2+3] trace	[1+2+3] few	[1+2] few	**[1+3] many**	**2/4/2**	**[3] many**	[1] trace + 2
7/1	clear solution	[1+2+3] trace	clear solution	[1+3] few	**3/2/3**	3+ impurities	**[2] few**
8/0	clear solution	clear solution	clear solution	clear solution	**3/3/2**	[3] few + impurities	2+ impurities

Note: The powder means that we can not get any crystals, but there may be some products.

The impurities are precipitation among crystals, which are obviously different from crystals.

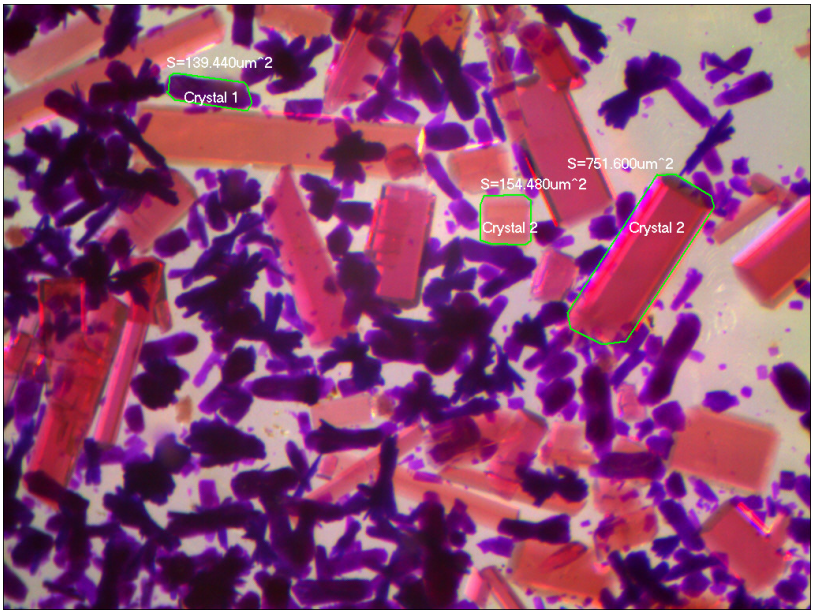

Fig. S18. The optical microscope photographs of two-component crystals **1** and **2.**

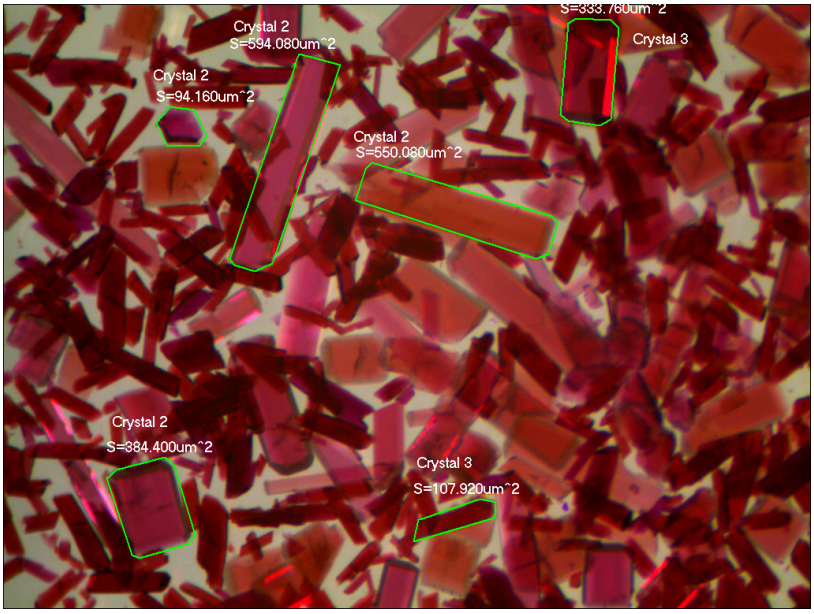

Fig. S19. The optical microscope photographs of two-component crystals **2** and **3.**

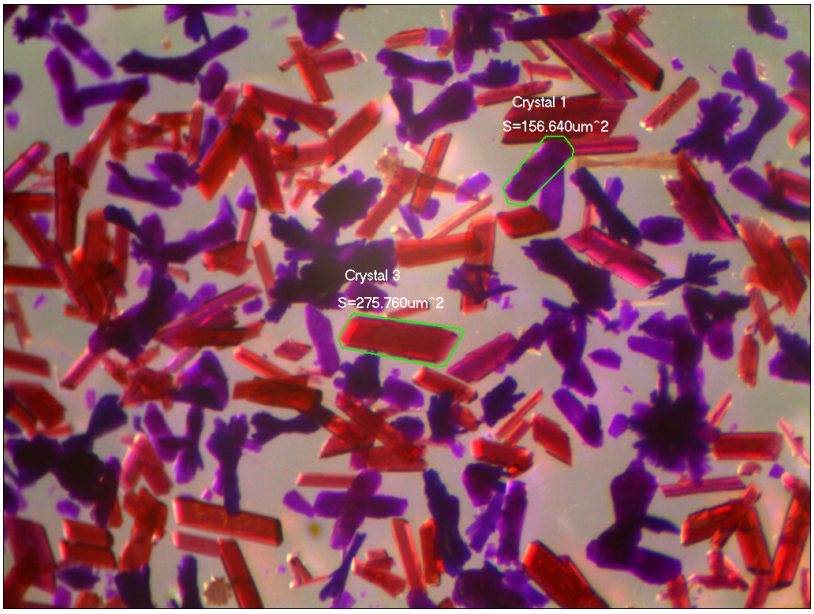

Fig. S20. The optical microscope photographs of two-component crystals **1** and **3.**

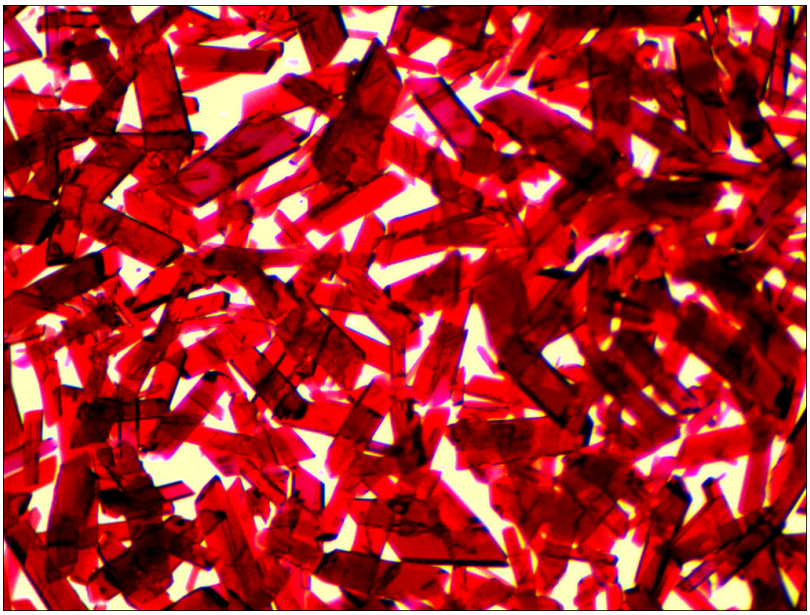

Fig. S21. The optical microscope photographs of one-component crystals **3.**

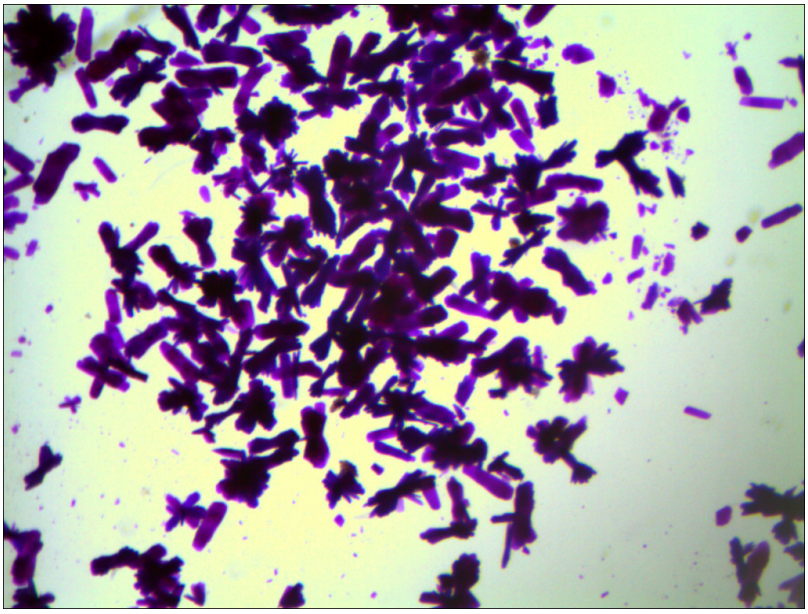

Fig. S22. The optical microscope photographs of one-component crystals **1**

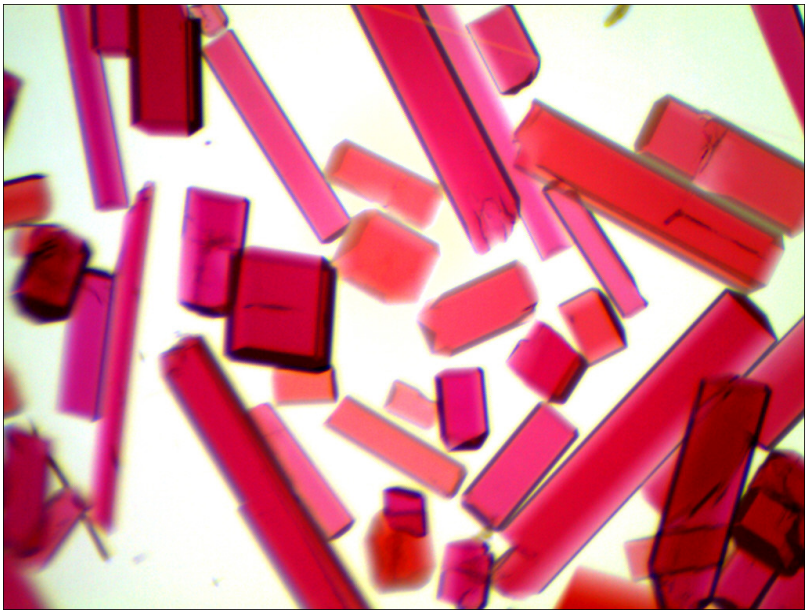

Fig. S23. The optical microscope photographs of one-component crystals **2**

References

1. L. Jiang, X. R. Meng, H. Xiang, P. Ju, D. C. Zhong and T. B. Lu, *Inorg. Chem.* 2012, **51**, 1874.
2. International Tables for X-Ray Crystallography; Kynoch Press:Birmingham, England, 1952; Vol. III.
3. SAINT, version 6.02; Bruker AXS: Madison, WI, 1999.
4. Sheldrick, G. M. SADABS: Empirical Absorption Correction-Program; University of Göttingen: Göttingen, Germany, 1997.
5. XPREP, version 5.1; Siemens Industrial Automation Inc.: Madison, WI, 1995.
6. Sheldrick, G. M. SHELXTL Reference Manual, version 5.1; Bruker AXS: Madison, WI, 1997.
7. Sheldrick, G. M. SHELXL-97: Program for Crystal Structure Refinement; University of Gottingen: Gottingen, Germany, 1997.
8. M. J. Frisch, G. W. Trucks, H. B. Schlegel, G. E. Scuseria, M. A. Robb, J. R. Cheeseman, G. Scalmani, V. Barone, B. Mennucci, G. A. Petersson, H. Nakatsuji, M. Caricato, X. Li, H. P. Hratchian, A. F. Izmaylov, J. Bloino, G. Zheng, J. L. Sonnenberg, M. Hada, M. Ehara, K. Toyota, R. Fukuda, J. Hasegawa, M. Ishida, T. Nakajima, Y. Honda, O. Kitao, H. Nakai, T. Vreven, J. A. Jr. Montgomery, J. E. Peralta, F. Ogliaro, M. Bearpark, J. J. Heyd, E. Brothers, K. N. Kudin, V. N. Staroverov, T. Keith, R. Kobayashi, J. Normand, K. Raghavachari, A. Rendell, J. C. Burant, S. S. Iyengar, J. Tomasi, M. Cossi, N. Rega, J. M. Millam, M. Klene, J. E. Knox, J. B. Cross, V. Bakken, C. Adamo, J. Jaramillo, R. Gomperts, R. E. Stratmann, O. Yazyev, A. J. Austin, R. Cammi, C. Pomelli, J. W. Ochterski, R. L. Martin, K. Morokuma, V. G. Zakrzewski, G. A. Voth, P. Salvador, J. J. Dannenberg, S. Dapprich, A. D. Daniels, O. Farkas, J. B. Foresman, J. V. Ortiz, J. Cioslowski and D. J. Fox, Gaussian 09, Revision B.01, Gaussian, Inc.: Wallingford, CT, 2010.
9. Y. Zhao and D. G. Truhlar, *Theor. Chem. Acc.* 2008, **120**, 215.
10. (a) P. J. Hay and W. R. J. Wadt, *Chem. Phys.* 1985, **82**, 270; (b) W. R. Wadt and P. J. Hay, *J. Chem. Phys.* 1985, **82**, 284; (c) P. J. Hay and W. R. Wadt, *J. Chem. Phys.* 1985, **82**, 299.